Revista Mexicana de Astronomía y Astrofísica, **44**, 293–300 (2008)

THE INTERACTION OF A YSO OUTFLOW WITH THE SURROUNDING MOLECULAR CLOUD CORE

J. Cantó,[1] A. C. Raga,[2] and D. A. Williams[3]

Received 2008 March 14; accepted 2008 June 23

RESUMEN

Presentamos un modelo analítico de capa delgada para un flujo eyectado con un ángulo de apertura que crece en función del tiempo. Este modelo predice una cavidad que se ensancha con el tiempo, y que se estrangula sobre el eje del flujo en un punto que se aleja de la fuente. La motivación de este modelo son las observaciones de una cavidad bipolar centrada en Barnard 5 IRS 1 de Velusamy & Langer (1998), quienes sugieren una interpretación de la estructura observada con un modelo como el que hemos desarrollado. Encontramos que la estructura observada sí puede ser producida por un flujo con colimación decreciente en función del tiempo, para una pérdida de masa del flujo de $\dot{M}_0 \approx 3 \times 10^{-6} M_\odot$ yr^{-1}.

ABSTRACT

We present a thin shell, analytic model for an outflow ejected with an opening angle that increases as a function of time. This model predicts a cavity shape that broadens out with time, and pinches towards the outflow axis at a point that travels away from the outflow source. The motivation for this model is the set of observations of a bipolar cavity centered on Barnard 5 IRS 1 by Velusamy & Langer (1998), who suggest an interpretation for the observed structure in terms of a model such as the one that we have studied. We find that this observed structure could indeed be produced by an outflow of decreasing collimation as a function of time, provided that the mass loss rate has a value $\dot{M}_0 \approx 3 \times 10^{-6} M_\odot$ yr^{-1}.

Key Words: ISM: jets and outflows — ISM: kinematics and dynamics — stars: mass loss — stars: pre-main sequence

1. INTRODUCTION

There is considerable observational evidence for the interaction of a jet from a young stellar object (YSO) with the dense core within which the YSO formed. Early indications of such an interaction were the detection of HCO^+ emission from unresolved dense cores which implied an HCO^+ abundance an order of magnitude larger than could be sustained in the physical conditions of the core itself (e.g. Gregersen et al. 1997; Ward-Thompson & Buckley 2001; Rawlings & Yates 2001). Rawlings, Taylor, & Williams (2000) suggested that a significantly enhanced abundance of HCO^+ might arise in the interface at the boundary of the cavity created by the emerging jet in the dense core through an interaction between ionised wind gas and molecular gas; the reaction of C^+ with H2O released from the dust grains of the core creates HCO^+ directly. Viti, Natarajan, & Williams (2002) showed that a variety of other molecules, other than HCO^+, should also be enhanced in the interface.

The morphology of the interaction may in some cases be directly observable. Hogerheijde et al. (1998) observed HCO^+ emission in several dense star-forming cores of which one, L1527, shows a "butterfly" morphology with an opening angle of about 90 degrees. These authors interpreted this structure as arising from enhanced abundance of HCO^+ in the wall of the cavity created by the jet/core interaction. Rawlings et al. (2004) used a radiative transfer code to show that such a model would indeed present the morphology observed by Hogerheijde et al. (1998). More convincing obser-

[1]Instituto de Astronomía, Universidad Nacional Autónoma de México, Mexico.
[2]Instituto de Ciencias Nucleares, Universidad Nacional Autónoma de México, Mexico.
[3]Department of Physics and Astronomy, University College London, UK.

vations of the morphology of a jet/core cavity were made by Velusamy & Langer (1998) in their study of Barnard 5 IRS1, an embedded YSO with bipolar molecular outflows. They inferred that the interaction created a near-parabolic cavity, and that this implied that the opening angle at the base of the jet was increasing and would be fully open in about 10^4 yr. Thus, cavity morphology may be a guide to the evolutionary age of the jet.

In the present paper, we apply the thin-shell formalism of Cantó, Raga, & Adame (2006) to the problem of an outflow with an initial opening angle that increases with time, travelling into a stratified environment. Four different analytical solutions (for winds with a constant mass loss rate per unit solid angle and with a constant total mass loss rate, moving into a uniform environment or into an environment with a R^{-2} radial density law) are described in §§ 2–4. In § 5, we apply one of these solutions (the one for a constant mass loss rate outflow moving into a stratified environment) for modelling the Barnard 5 IRS1 outflow and cavity. This study demonstrates the ready applicability of the theory, showing that the precise morphology and specific evolutionary timescale arise naturally from the jet/core interaction, for plausible choices of the physical parameters of the region. The implications of these results are briefly discussed in § 6.

2. THE MODEL

We consider a jet which is ejected from a source along the z-axis of a cylindrical coordinate system centered on the source. The jet decollimates as a function of time at a constant rate ϵ, so that the half-opening angle of the ejection at time τ is $\theta_j = \epsilon\tau$. We assume that the ejection velocity v_0 is isotropic (i. e., is independent of the ejection angle) within the jet beam, and constant in time as the opening angle at the base of the jet widens.

For the mass loss rate we consider two cases:

1. a mass loss rate per unit solid angle $\dot{m}_0$ which remains constant in time, and
2. a time-independent total mass loss rate $\dot{M}_0$.

In the first case, the total mass loss rate in the jet increases with time, while in the second case the mass loss rate per unit solid angle decreases for increasing times.

For a given ejection time τ and angle θ (measured out from the z-axis), the jet velocity and mass loss rate per unit solid angle can be expressed as

$$v_j = v_0\, s(\theta,\tau), \quad \text{and} \quad \dot{m}_j = \dot{m}_0(\tau)\, s(\theta,\tau)\,, \qquad (1)$$

where $s(\theta,\tau)$ is the step function

$$\begin{aligned} s(\theta,\tau) &= 1 \,\text{for}\, 0 \le \theta \le \epsilon\tau\ ; \\ s(\theta,\tau) &= 0 \,\text{for}\, \epsilon\tau < \theta \le \pi/2\,. \end{aligned} \qquad (2)$$

The interaction of the jet with the surrounding medium forms an expanding shell moving radially away from the star. Following Cantó et al. (2006), the position $R_S(\theta,t)$ of the shell at time t in the direction θ is given by the solution of the equations:

$$R_S(\theta,t) = (t-\tau) v_j(\theta,\tau)\,, \qquad (3)$$

$$(I_1 + I_5)\, R_S - I_2 t + I_3 - I_6 = 0\,, \qquad (4)$$

where $\tau(\theta)$ is the ejection time of the jet material which at time t is entering the shell in the θ-direction, and

$$I_1(\theta,\tau) \equiv \int_0^\tau \dot{m}_j(\theta,\tau')\, d\tau'\,, \qquad (5)$$

$$I_2(\theta,\tau) \equiv \int_0^\tau \dot{m}_j(\theta,\tau')\, v_j(\theta,\tau')\, d\tau'\,, \qquad (6)$$

$$I_3(\theta,\tau) \equiv \int_0^\tau \dot{m}_j(\theta,\tau')\, v_j(\theta,\tau')\, \tau'\, d\tau'\,, \qquad (7)$$

$$I_5(\theta,R_S) \equiv \int_0^{R_S} \rho_a(\theta,R)\, R^2\, dR\,, \qquad (8)$$

$$I_6(\theta,R_S) \equiv \int_0^{R_S} \rho_a(\theta,R)\, R^3\, dR\,. \qquad (9)$$

In equations (8) and (9), $\rho_a(\theta,R)$ represents the density distribution of the surrounding medium, which may be a function of the distance R from the star as well as of the direction θ.

Substituting equations (1) and (2) into (3), we then obtain:

$$R_S(\theta,t) = (t-\tau) v_0\,; \quad \theta \le \epsilon\tau\,, \qquad (10)$$

$$R_S(\theta,t) = 0\,; \quad \theta > \epsilon\tau\,. \qquad (11)$$

In order to proceed further, it is necessary to specify the angular and time dependence of the ejected wind, as well as the spatial dependence of the ambient density. Different possible choices are explored in the two following sections.

3. JET WITH CONSTANT MASS LOSS RATE PER UNIT SOLID ANGLE

Let us consider the case of a mass loss rate per unit solid angle $\dot{m}_0$ which is constant in time and uniform within the jet beam. Using equations (1),

(2), and (5–7) we obtain

$$I_1 = \left(\tau - \frac{\theta}{\epsilon}\right) \dot{m}_0 \,, \quad (12)$$

$$I_2 = \left(\tau - \frac{\theta}{\epsilon}\right) \dot{m}_0 v_0 \,, \quad (13)$$

$$I_3 = \frac{1}{2}\left(\tau^2 - \frac{\theta^2}{\epsilon^2}\right) \dot{m}_0 v_0 \,, \quad (14)$$

for $\theta \leq \epsilon\tau$ and zero otherwise.

Substituting (10–14) into (4), we obtain

$$t = \frac{\theta}{\epsilon} + \frac{R_S}{v_0} + \sqrt{\frac{2}{\dot{m}_0 v_0}\left(R_S I_5 - I_6\right)} \,, \quad (15)$$

which relates the shell radius R_S, the angle θ and the time t. Note that equation (15) is only valid for angles $\theta \leq \epsilon\tau = \theta_m$, and that $R_S = 0$ for $\theta > \theta_m$.

We should note that if one takes the $\epsilon \to \infty$ limit (i. e., the jet instantaneously increases its opening angle to become isotropic), equation (15) coincides with the isotropic wind solution of Cantó et al. (2006). It also follows from equation (15) that the solution for the interaction of a jet with increasing opening angle (as a function of time) and constant velocity and mass loss rate per unit solid angle is the solution for the shell pushed out by a steady wind, but with a time delay θ/ϵ for a given direction θ. This delay represents the time for the lateral boundary of the jet cone to reach the angle θ and start blowing out the shell in this direction.

Let us now consider two possibilities for the environmental distribution: a uniform density $\rho_a = \rho_0$ and an outwardly decreasing density of the form $\rho_a = \kappa/R^2$ (with κ independent of distance R from the source but with a possible dependence on θ).

i. Uniform environment ($\rho_a = \rho_0$)

From equations (8) and (9) we obtain

$$I_5 = \frac{1}{3}\rho_0 {R_S}^3 \,, \quad (16)$$

$$I_6 = \frac{1}{4}\rho_0 {R_S}^4 \,. \quad (17)$$

Substituting (16) and (17) into equation (15) we then obtain

$$R_S = \frac{R_0}{\sqrt{2}}\left[\sqrt{3 + 2\sqrt{6}\left(t - \frac{\theta}{\epsilon}\right)\frac{v_0}{R_0}} - \sqrt{3}\right] \,, \quad (18)$$

where

$$R_0 \equiv \sqrt{\frac{\dot{m}_0}{\rho_0 v_0}} \,. \quad (19)$$

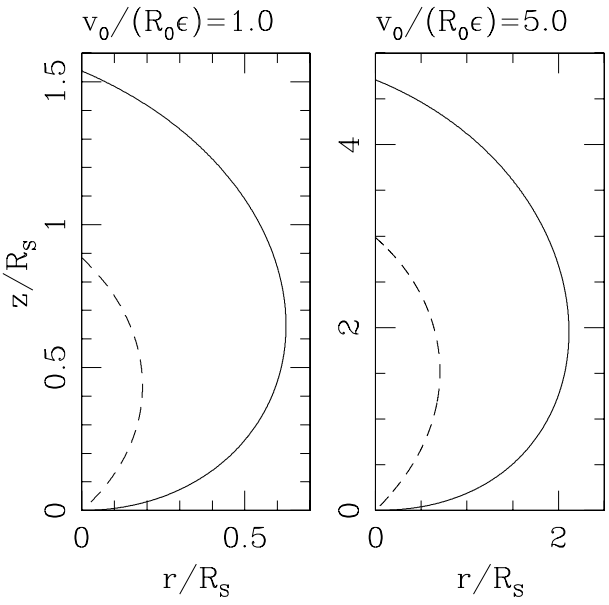

Fig. 1. Cavity shapes obtained from the constant mass loss rate per unit solid angle, uniform environment model. The left frame shows the cavities obtained for a model with $v_0/(R_0\epsilon) = 1.0$, and the right hand frame for a model with $v_0/(R_0\epsilon) = 5.0$. For both models we show the cavities for times $\epsilon t = \pi/4$ (dashed curves) and $\epsilon t = \pi/2$ (solid curves).

The cavity shapes that are produced by equation (18) open out from the position of the source, and eventually curve back towards the symmetry axis, ending in a pointed apex, as can be seen from the two examples shown in Figure 1.

ii. Power law environment ($\rho_a = \kappa/R^2$)

From equations (8) and (9) we obtain

$$I_5 = \kappa R_S \,, \quad (20)$$

$$I_6 = \frac{1}{2}\kappa {R_S}^2 \,. \quad (21)$$

Substituting (20) and (21) into equation (15) we then obtain

$$R_S = \frac{v_0}{1 + \sqrt{A}}\left(t - \frac{\theta}{\epsilon}\right) \,, \quad (22)$$

where

$$A \equiv \frac{\kappa v_0}{\dot{m}_0} \,, \quad (23)$$

which is constant along the radial direction, but could have a dependence on θ (because κ can have a θ-dependence).

As expected, the radius in this case increases with time at a constant velocity

$$v_S = \frac{v_0}{1 + \sqrt{A}} \,, \quad (24)$$

possibly dependent on direction (through the dependence of κ and A on θ, see above).

Figure 2 shows the solution obtained from equation (22) for a time such that the opening angle of the conical outflow is $\theta_m = 60°$.

4. JET WITH CONSTANT TOTAL MASS LOSS RATE

In this case, the mass loss rate per unit solid angle decreases with time as

$$\dot{m}_0 = \frac{\dot{M}_0}{\Omega(\tau)}\,, \tag{25}$$

where $\dot{M}_0$ is the total mass loss rate and

$$\Omega(\tau) = 2\pi\left[1 - \cos(\epsilon\tau)\right]\,, \tag{26}$$

is the solid angle (subtended by the opening angle θ) of the jet at ejection time τ. Combining equations (25) and (26) with (5–7) one obtains:

$$I_1 = \frac{\dot{M}_0}{2\pi\epsilon}\left[\mathrm{cotan}\left(\frac{\theta}{2}\right) - \mathrm{cotan}\left(\frac{\epsilon\tau}{2}\right)\right]\,, \tag{27}$$

$$I_2 = \frac{\dot{M}_0 v_0}{2\pi\epsilon}\left[\mathrm{cotan}\left(\frac{\theta}{2}\right) - \mathrm{cotan}\left(\frac{\epsilon\tau}{2}\right)\right]\,, \tag{28}$$

$$I_3 = \frac{\dot{M}_0 v_0}{2\pi\epsilon^2}\left\{\theta\ \mathrm{cotan}\left(\frac{\theta}{2}\right) - \epsilon\tau\ \mathrm{cotan}\left(\frac{\epsilon\tau}{2}\right) + 2\ \ln\left[\frac{\sin(\epsilon\tau/2)}{\sin(\theta/2)}\right]\right\}. \tag{29}$$

i. Uniform environment ($\rho_a = \rho_0$)

The integrals I_5 and I_6 are given by equations (16) and (17). Substituting the results of these integrals, together with (10) and (27–29) into equation (4) one obtains:

$$\epsilon^2\pi\rho_0 {R_S}^4 + 6\dot{M}_0\left[\theta v_0 + \epsilon(R_S - t v_0)\right]\mathrm{cotan}\left(\frac{\theta}{2}\right) + 12\dot{M}_0 v_0 \ln\left\{\frac{\sin\left[\epsilon(t - R_S/v_0)/2\right]}{\sin(\theta/2)}\right\} = 0\,, \tag{30}$$

which gives, in an implicit way, the radius of the shell as a function of θ (in the interval $0 \le \theta \le \epsilon t$) for a given time t.

We note that equation (30) gives (correctly) that $R_S = 0$ for $\theta = \epsilon t$, which is the opening angle of the jet at time t. It also follows from equation (30) that $R_S = v_0 t$ for $\theta = 0$ at any time. This is a result of the fact that initially (i. e., at $t = 0$) the jet has a zero opening angle, and its density is infinite. Under this condition the medium presents no resistance to the jet motion, and therefore the perturbation driven by the initial ejection travels ballistically at the ejection velocity v_0.

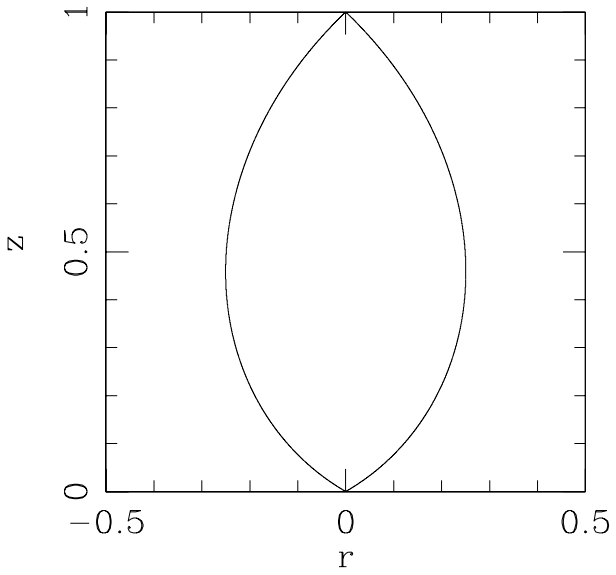

Fig. 2. Cavity shape obtained from the constant mass loss rate per unit solid angle, $\rho_a = \kappa/R^2$ environment model. The displayed shape corresponds to a maximum opening angle $\theta_m = 60°$, and the (z, r) coordinates have been normalized to the axial extent of the cavity.

Finally, we can write equation (30) in dimensionless form. To do this, we first define:

$$\theta_m \equiv \epsilon t\,, \tag{31}$$

$$\overline{R_S} \equiv R_S/R_0\,, \tag{32}$$

$$\overline{\rho_0} \equiv \frac{\pi\rho_0 v_0 {R_0}^2}{\dot{M}_0}\,, \tag{33}$$

$$\overline{\epsilon} \equiv \frac{\epsilon R_0}{v_0}\,, \tag{34}$$

where R_0 is a characteristic length. Equation (30) can then be written as

$$\overline{\epsilon}^2\overline{\rho_0}\,\overline{R_S}^4 + 6\left(\overline{\epsilon}\,\overline{R_S} + \theta - \theta_m\right)\mathrm{cotan}\left(\frac{\theta}{2}\right) + 12\ \ln\left\{\frac{\sin\left[(\theta_m - \overline{\epsilon}\,\overline{R_S})/2\right]}{\sin(\theta/2)}\right\} = 0\,. \tag{35}$$

With the definitions above, we have

$$\overline{R_S}(\theta = 0) = \frac{\theta_m}{\overline{\epsilon}}\,. \tag{36}$$

ii. Power law environment ($\rho_a = \kappa/R^2$)

In this case, the integrals (8) and (9) are given by equations (20) and (21). Using the results from these integrals, together with equations (4) and (27–29), we obtain:

$$\epsilon^2 \kappa \pi {R_S}^2 + \dot{M}_0 \left[\theta v_0 + \epsilon \left(R_S - t v_0\right)\right] \text{ cotan}\left(\frac{\theta}{2}\right)$$

$$+2\dot{M}_0 v_0 \ \ln\left\{\frac{\sin\left[\epsilon(t - R_S/v_0)/2\right]}{\sin(\theta/2)}\right\} = 0\,. \qquad (37)$$

As in the uniform density case, equation (37) gives $R_S = 0$ for $\theta = \epsilon t$, and $R_S = v_0 t$ for $\theta = 0$ for any time t.

Finally, we can write equation (37) in dimensionless form. To do this, we first define:

$$\overline{\kappa} \equiv \frac{4\pi\kappa v_0}{\dot{M}_0}\,. \qquad (38)$$

Also using the definitions in equations (31–34), equation (37) can then be written as

$$\overline{\epsilon}^2 \overline{\kappa} {\overline{R_S}}^2 + 4\left(\overline{\epsilon}\overline{R_S} + \theta - \theta_m\right) \text{ cotan}\left(\frac{\theta}{2}\right)$$

$$+8 \ln\left\{\frac{\sin\left[(\theta_m - \overline{\epsilon}\overline{R_S})/2\right]}{\sin(\theta/2)}\right\} = 0\,. \qquad (39)$$

The solutions given by equations (35) and (39) both correspond to cavities that first open out from the position of the source, and then converge onto the symmetry axis forming a pointed, axially pinched structure. We show these shapes in more detail in the following section (also see Figures 3 and 4), in which we attempt to compare these two solutions with the observed shape of IRS 1 in Barnard 5.

5. AN APPLICATION TO IRS 1 IN BARNARD 5

Barnard 5 is a dark molecular cloud NE of NGC 1333 at a distance $D = 350$ pc. It has a size of $\sim 6 \times 3$ pc and a total mass of $\sim 1000\ M_\odot$. The IRAS survey resulted in the detection of four point sources, the most luminous of them (IRS 1) having an infrared luminosity of $\sim 10\ L_\odot$ (Beichman et al. 1984).

Goldsmith, Langer, & Wilson (1986) detected a bipolar, high-velocity ($\Delta v \sim 30$ km s^{-1}) molecular outflow associated with IRS 1. Fuller et al. (1991) confirmed the presence of this outflow and presented a high resolution map of the region, showing that it has an extent of at least 0.3 pc and is oriented along a $PA \sim 60°$. However, Bally, Devine, & Alten (1996) reanalyzed the Goldsmith et al. (1986) data and concluded that the high-velocity molecular gas extends from IRS 1 to the E and W ends of a newly detected parsec-scale Herbig-Haro jet also emerging from this source. The brightest part of the blueshifted jet is at a position angle of $\sim 75°$, has a velocity of ~ 100 km s^{-1} and is located at about $660''$ (~ 1.1 pc) from IRS 1.

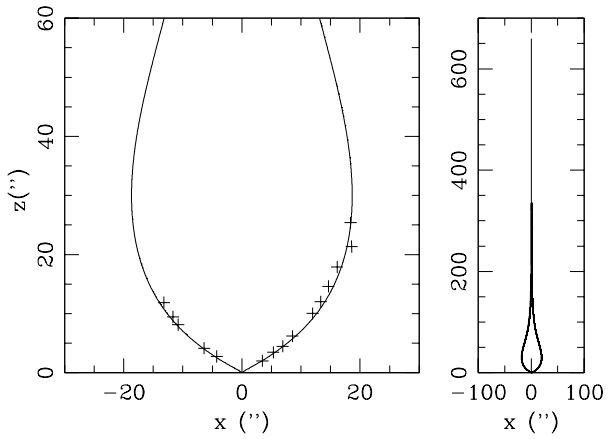

Fig. 3. Cavity obtained from the fit of our constant mass loss rate, constant ρ_a model to the observations of the NE cavity of Barnard 5 IRS 1. The left frame shows the base of the cavity (with distance measured in arcseconds from the position of the outflow source) predicted from the model (solid line), superimposed on the observed positions (see Table 1) of the maxima along the NE cavity (crosses). The right frame shows the shape of the predicted cavity, extending out to the position in which HH objects are observed.

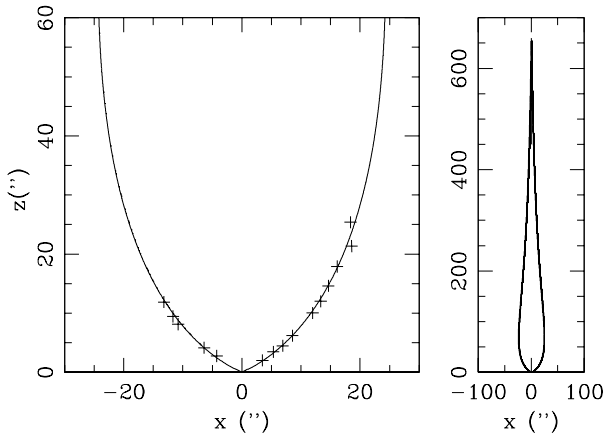

Fig. 4. Cavity obtained from the fit of our constant mass loss rate, $\rho_a = \kappa/R^2$ model to the observations of the NE cavity of Barnard 5 IRS 1. The left frame shows the base of the cavity and the right frame shows the full shape of the predicted cavity (see also Figure 3).

Langer, Velusamy, & Xie (1996) and Velusamy & Langer (1998) present interferometric, high-resolution images of the inner part ($\pm 20''$ from the source) of the molecular outflow. They show that the outflow consists of two cone-like features originating in IRS 1, the blue one fanning open to the NE and the red one to the SW. The cone axis is oriented at a 73° position angle, which is close to the direction of the optical jet. Also, the outflow lobes are parabolic near the vertices, and show a strong, limb-brightened emission, interpreted as a biconical cavity with walls that appear to be pushing and compressing the ambient gas. Velusamy & Langer (1998) suggest that all of these features can be interpreted in terms of an increase in the opening angle of the outflow cone as a function of time.

In order to apply our models to the outflow described above, we start by measuring the position angle and the distances from the star to the most prominent local maxima along the N and S arms of the intensity map of the blueshifted lobe (shown in Figure 3 of Velusamy & Langer 1998). We find that the angle θ between the symmetry axis and the line connecting these maxima with the star and their distance R_S (from the star) have a strong linear correlation. We then fit the data with a relation

$$R_S \approx a + b\theta\,, \tag{40}$$

where $\theta = |PA - PA_S|$ (PA being the position angle of the intensity maxima and PA_S being the position angle of the symmetry axis) and a and b are constants. We then carry out a simple minimization procedure, from which we obtain $PA_S = 73\overset{\circ}{.}03$ which is actually very close to the value estimated by Langer et al. (1996). We should note that essentially the same result for PA_S is obtained by fitting a quadratic polynomial in θ to the data.

With this $PA_S = 73\overset{\circ}{.}03$ value we then rotate the observations in such a way that the symmetry axis lies along the z-axis of a Cartesian reference frame, with its y-axis pointing towards the observer and x-axis on the plane of the sky. The (x, z) coordinates (in seconds of arc) of the maxima delineating the cavity walls are given in Table 1, and are plotted in Figure 1. In Table 1, we also give the angle θ and distance to the source R_S of the maxima.

We now model this cavity with our solutions for a constant $\dot{M}_0$ outflow moving into a constant density medium or into a $\rho_a = \kappa/R^2$ stratified environment (see §§ 4. *i* and 4. *ii*). These two solutions appear to be appropriate because they produce axially pinched structures which are consistent with the fact that one observes HH objects concentrated to the outflow axis at $\approx 660''$ from the source (see above and Bally et al. 1996). The two constant mass loss rate per unit solid angle solutions produce flat topped cavity shapes which are qualitatively inconsistent with this observation (see §§ 3. *i* and 3. *ii*).

TABLE 1

SHAPE OF THE CAVITY

Maxima	$R_S('')$	$\theta(^\circ)$	$x('')$	$z('')$
N1	31.27	36.03	18.39	25.39
N2	28.31	41.03	18.58	21.36
N3	24.08	42.03	16.12	17.89
N4	20.70	45.03	14.65	14.63
N5	17.96	48.03	13.35	12.01
N6	15.63	50.03	11.98	10.04
N7	10.56	54.03	8.55	6.20
N8	6.34	57.03	5.32	3.45
N9	8.24	57.02	6.91	4.48
N10	4.01	60.03	3.48	2.01
S1	17.75	47.97	−13.18	11.88
S2	15.00	50.97	−11.65	9.45
S3	13.52	52.97	−10.79	8.14
S4	7.61	56.97	−6.38	4.15
S5	5.07	56.97	−4.25	2.76

We first assume that the observed outflow axis lies on the plane of the sky. We consider $R_0 = 1''$ (i.e., distances measured in arcseconds) and $\overline{R_S}(\theta = 0) = 660$ (see above and equation 36).

We then carry out fits of the predicted shapes (equations 35 and 39) to the data (see Table 1). For the model of a constant mass loss rate flow moving into a constant density environment (see § 4.*i* and equation 35), we obtain $\overline{\rho_0} = 0.65$ $\overline{\epsilon} = 1.60 \times 10^{-3}$ and $\theta_m = 60\overset{\circ}{.}2$. This fit is shown together with the measured cavity shape in Figure 3. In this figure, we also show the predicted shape of the outflow cavity, which extends away from the source and pinches at the position of the observed HH objects.

From the fit with the constant mass loss rate, power law environment model (see § 4.*i* and equation 39), we obtain $\overline{\kappa} = 460$, $\overline{\epsilon} = 1.74 \times 10^{-3}$ and $\theta_m = 66\overset{\circ}{.}0$. This fit is shown together with the measured cavity shape in Figure 4.

If we now assume that the outflow has a velocity $v_0 = 100$ km s^{-1}, we then determine an evolutionary time $t = 1.1 \times 10^4$ yr and an opening rate $\epsilon \approx 6 \times 10^{-3}$ deg yr^{-1} for the outflow. This value of ϵ coincides with the opening rate estimated by Velusamy & Langer (1998).

Let us now concentrate on the model with the ρ_a=κ/R^2 environmental density distribution, which appears to be more realistic for modelling an object which is formed in the middle of a molecular cloud core. Fuller et al. (1991) found three dense clumps around IRS1, with a total mass of 0.55 $M_\odot$ within a radius of $\sim 1.3\times10^{17}$ cm. If these knots represent the inner part of the κ/R^2 density distribution around the outflow source, the observationally determined mass implies that $\kappa \approx 6.7 \times 10^{14}$ g cm^{-1}. Then, using this value of κ and the definition of $\overline{\kappa}$ (see equation 38), the $\overline{\kappa} = 460$ value determined from the fit to the observed cavity shape (see above and Figure 1) and the assumed $v_0 = 100$ km s^{-1} outflow velocity we derive an outflow mass loss rate of $\dot{M}_0 \approx 3 \times 10^{-6}$ $M_\odot$ yr^{-1}. This mass loss rate compares well with estimates of $\dot{M}_0$ for other young stars with collimated outflows.

6. CONCLUSIONS

We have derived an analytic, thin shell model for an outflow ejected with an opening angle that increases with time, travelling into a homogeneous or a stratified ($\rho_a \propto R^{-2}$) environment. We have derived full solutions for outflows with a constant mass loss rate per unit solid angle $\dot{m}_0$ (§ 3) and with a constant total mass loss rate $\dot{M}_0$ (§ 4).

This study has been motivated by the interferometric observations of Velusamy & Langer (1998) of a bipolar cavity structure centered on Barnard 5 IRS 1. Bally et al. (1996) also discovered a giant HH outflow ejected by the same source. Velusamy & Langer (1998) interpreted the observed cavity as evidence of an outflow ejected with an opening angle that increases with time.

We find that while constant $\dot{m}_0$ models produce cavities with a broad head (§ 3), constant $\dot{M}_0$ models (§ 4) produce cavity structures which end in a pinched, collimated structure extending away from the source along the symmetry axis. The constant $\dot{M}_0$ models are therefore more interesting for modelling objects such as IRS 5 in Barnard 5, which has an extended cavity structure close to the source and a more collimated, jet-like structure at larger distances.

We have applied our dynamical models of a constant $\dot{M}_0$ outflow moving into a constant density environment and into a $\rho_a \propto R^{-2}$ density distribution to the observations of this outflow. We find that for both models one can choose parameters such that both the shape of the observed cavity and the distance to the end of the giant HH flow (which in our model would correspond to the top of the pinched cavity) are reproduced by the model. This agreement between the observations and the morphology predicted by the model is obtained for an outflow with an evolutionary timescale of $\approx 1.1 \times 10^4$ yr and an opening rate $\epsilon = 6 \times 10^{-3}$deg yr^{-1} (assuming a $v_0 = 100$ km s^{-1} outflow velocity, see § 5). Furthermore, considering the $\rho_a \propto R^{-2}$ model, we can normalize the environmental density stratification to the mass around IRS 1 determined by Fuller et al. (1991), and then obtain $\dot{M}_0 \approx 3 \times 10^{-6}$ $M_\odot$ yr^{-1} for the mass loss rate of the outflow.

Therefore, we conclude that the model proposed by Velusamy & Langer (1998) for explaining the Barnard 5 IRS 1 cavity (in terms of the action of an outflow with an opening angle that increases with time) survives a more detailed, dynamical analysis. Our model shows that an outflow with a reasonable ejection velocity and mass loss rate (and with the $\epsilon = 6 \times 10^{-3}$ deg yr^{-1} opening rate deduced by Velusamy & Langer 1998) would indeed produce the observed cavities.

In this paper, we have presented four different, fully analytic models for shells driven by a jet with an increasing opening angle as a function of time. In order to illustrate the possible use of our models, we have carried out a comparison with the Barnard 5 IRS 1 cavity. The models of course are also useful for attempting to model other cavity structures centered on YSO's. Several examples of this kind of structure have been observed by Arce & Sargent (2006), who also present an interpretation of the observed structures as the result of outflows with opening angles that grow with time. A future comparison between our models and the morphologies and kinematics of the cavities observed by Arce & Sargent (2006) might provide useful insights regarding the time-evolution of outflows from YSO's.

JC and AR acknowledge support from the DGAPA (Universidad Nacional Autónoma de México) grant IN108207, from the Conacyt grants 46828-F and 61547, and from the "Macroproyecto de Tecnologías para la Universidad de la Información y la Computación" (Secretaría de Desarrollo Institucional de la Universidad Nacional Autónoma de México). We thank an anonymous referee for helpful comments.

REFERENCES

Arce, H. G., & Sargent, A. I. 2006, ApJ, 646, 1070
Bally, J., Devine, D., & Alten, V. 1996, ApJ, 473, 921
Beichman, C. A., et al. 1984, ApJ, 278, L45
Cantó, J., Raga, A. C., & Adame, L. 2006, MNRAS, 369, 860

Fuller, G. A., et al. 1991, ApJ, 376, 135
Goldsmith, P. F., Langer, W. D., & Wilson, R. W. 1986, ApJ, 303, L11
Gregersen, E. M., Evans, N. J., Zhou, S., & Choi, M. 1997, ApJ, 484, 256
Hogerheijde, M. R., van Dishoeck, E. F., Blake, G. A., & van Langevelde, H. J. 1998, ApJ, 502, 315
Langer, W. D., Velusamy, T., & Xie, T. 1996, ApJ, 468, L41
Rawlings, J. M. C., Taylor, S. D., & Williams, D. A. 2000, MNRAS, 313, 461
Rawlings, J. M. C., & Yates, J. A. 2001, MNRAS, 326, 1423
Rawlings, J. M. C., Redman, M. P., Keto, E., & Williams, D. A. 2004, MNRAS, 351, 1054
Velusamy, T., & Langer, W. D. 1998, Nature, 392, 685
Viti, S., Natarajan, S., & Williams, D. A. 2002, MNRAS, 336, 797
Ward-Thompson, D., & Buckley, H. D. 2001, MNRAS, 327, 955

J. Cantó: Instituto de Astronomía, Universidad Nacional Autónoma de México, Apdo. Postal 70-264, 04510 México, D.F., Mexico (canto@astroscu.unam.mx).
A. C. Raga: Instituto de Ciencias Nucleares, Universidad Nacional Autónoma de México, Apdo. Postal 70-543, 04510 México, D.F., Mexico (raga@nucleares.unam.mx).
D. A. Williams: University College London, Gower St., London, UK (daw@star.ucl.ac.uk).